Title: Cavity-Enabled Enhancement of Ultrafast Intramolecular Vibrational Redistribution over Pseudorotation

Authors: Teng-Teng Chen[1]†, Matthew Du[1]†, Zimo Yang[2], Joel Yuen-Zhou[1*], Wei Xiong[1,2,3*]

Affiliations:

[1]University of California, San Diego, Department of Chemistry and Biochemistry, La Jolla, CA

[2]University of California, San Diego, Materials Science and Engineering Program, La Jolla, CA

[3]University of California, San Diego, Department of Electrical and Computer Engineering, La Jolla, CA

* Corresponding author. Email: joelyuen@ucsd.edu (Joel Yuen-Zhou) and w2xiong@ucsd.edu (Wei Xiong)

†These authors contributed equally to this work.

Abstract: Vibrational Strong Coupling (VSC) between molecular vibrations and microcavity photons yields a few polaritons (light-matter modes) and many dark modes (with negligible photonic character). Although VSC is reported to alter thermally-activated chemical reactions, its mechanisms remain opaque. To shed light on this problem, we followed ultrafast dynamics of a simple unimolecular vibrational energy exchange in Fe(CO)5 under VSC, which showed two competing channels: pseudorotation and intramolecular vibrational-energy redistribution (IVR). We found that, under polariton excitation, energy exchange was overall accelerated, with IVR becoming faster and pseudorotation being slowed down. However, dark mode excitation revealed unchanged dynamics compared to outside of cavity, with pseudorotation dominating. Thus, despite controversies of thermally-activated VSC modified chemistry, our work showed VSC can indeed alter chemistry upon non-equilibrium preparation of polaritons.

One-Sentence Summary: Vibrational polariton alters ultrafast molecular dynamics in liquid phase, and dark modes show no influences.

Vibrational strong coupling (VSC) gives rise to delocalized superpositions of molecular vibrations and electromagnetic modes (cavity modes), known as molecular vibrational polaritons(*1-3*). Recently, VSC has arisen as a promising handle to manipulate chemical reactions in condensed phases(*4-9*). Extensive experimental evidence has shown that, without photoexcitation, reaction rates can be either accelerated or decelerated by VSC, and reaction selectivity can even be altered(*4-6, 8*). Although much effort has been devoted to providing a sound explanation for VSC-modified chemistry, consensus between theory and experiments is still missing(*10-17*). Though it is clear that polaritons are different from bare molecular states, and thereby have the potential to modify chemistry, dark modes, which greatly outnumber polaritons, have the same excitation energies as the uncoupled vibrational modes(*18*). Hence, some theoretical work predicts that reactivity in the collective VSC regime is similar to that outside an optical cavity(*11, 13-15, 19, 20*), which is consistent with a couple of recent experimental results showing no modification of reactions from VSC(*16, 21*). Resolution of the discrepancies is hindered by the following factors: most reactions studied so far are quite complex, *i.e.*, involve multiple steps or are diffusion limited, and reactions involving both dark modes and polaritons are probed together(*4-8*). To delineate the effect of VSC, it is therefore critical to study elementary reactions and use a technique that can differentiate the contributions from polaritons and dark modes.

In this work, we used ultrafast two-dimensional infrared (2D IR) spectroscopy to follow how the polaritons and dark modes evolve in both pseudorotation and intramolecular energy redistribution (IVR) of $Fe(CO)_5$(*22*). We did so in a state-resolved manner, thereby meeting the desired criteria listed above. $Fe(CO)_5$ features two infrared (IR) active vibrational bands, a doubly degenerate e' mode at 1999 cm^{-1} involving three equatorial CO groups and an a_2" mode at 2022 cm^{-1} involving the axial CO groups (Fig. S1). Harris and co-workers applied 2D IR spectroscopy and showed that $Fe(CO)_5$ can rearrange from its D_{3h} equilibrium geometry to a C_{4v} transition state and back to D_{3h}, during which the equatorial and axial CO ligands interconvert, leading to vibrational energy exchange between a_2" and e' modes (*23*). This process, referred to as Berry's pseudorotation, is a single barrier crossing and thus represents the essence of elementary reactions, although the product is indistinguishable from the reactant(*24*). Given that Berry's pseudorotation competes with IVR between a_2" and e' modes whose transition dipoles are perpendicular to each other (Fig. 1A top), $Fe(CO)_5$ is an ideal testbed to understand how VSC affects single barrier crossing events and the branching ratio between various dynamical processes.

Using 2D IR spectroscopy, we found that, when polaritons were pumped, they could accelerate the overall 2D IR cross peak dynamics and, more interestingly, the excited polaritons make IVR faster than pseudorotation (Fig.1A bottom). In contrast, the dynamics triggered by exciting the dark reservoir modes were similar to the dynamics of molecules outside the cavity. Thus, the fundamental concept of VSC-modified chemistry – polaritons can change reactions – holds. However, because dark modes were statistically dominant, the overall influence of VSC on the dynamics of the $Fe(CO)_5$, when measured without differentiating polariton and dark modes (*e.g.*, without optical pumping at room temperature), should be negligible.

The VSC condition was achieved by placing a solution of $Fe(CO)_5$ in *n*-dodecane into a Fabry-Pérot microcavity. Unless specifically mentioned, we set the $Fe(CO)_5$ concentration to ~180 mM and the cavity longitudinal thickness to ~12.5 μm. The e' and a_2" vibrational modes of $Fe(CO)_5$ strongly couple to a 5^{th}-order cavity mode. The IR spectrum (Fig. 1B) shows the transitions of upper, middle, and lower polaritons (UP, MP and LP) at ω_{UP} = 2045, ω_{MP} = 2014, and ω_{LP} = 1976 cm^{-1}, respectively. By fitting to a coupled oscillator model (see Supplementary Materials (SM) Section 2.1), we determined that the cavity mode is 2013 cm^{-1} and it interacts with

the e' and a_2" modes with amplitudes $g_{cav\text{-}e'} = 26$ cm^{-1} and $g_{cav\text{-}a2"} = 19$ cm^{-1}, respectively. Because the full width at half maximum (FWHM) of the e' and a_2" modes are 8 cm^{-1} and 5 cm^{-1}, respectively, and that of the cavity mode is 11 cm^{-1}, the samples satisfy the criteria for VSC(*25*).

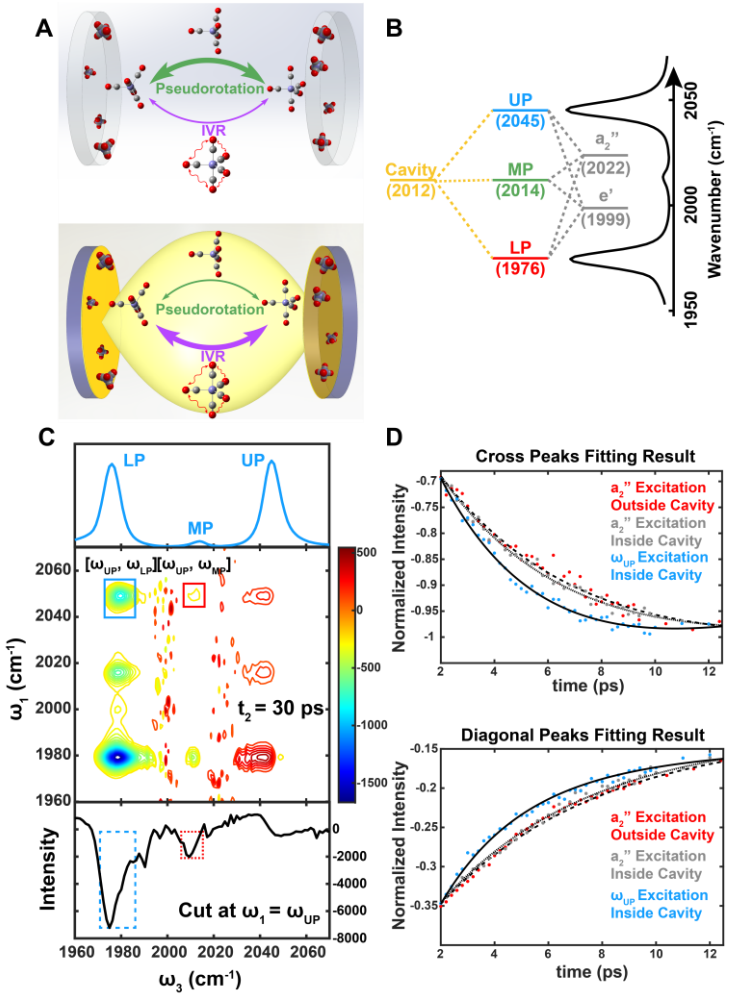

Fig. 1 Influence of VSC on $Fe(CO)_5$ energy exchange dynamics. (A) Schematic drawing showing that, when $Fe(CO)_5$ is outside of cavity, pseudorotation is the dominating channel (top); when the molecule is placed in an optical cavity, IVR becomes the dominant energy exchange process and pseudorotation is suppressed (bottom). (B) Strong coupling diagram and IR spectrum of $Fe(CO)_5$ inside the cavity. (C) Normalized 2D IR spectrum using linear spectrum of strongly coupled $Fe(CO)_5$ at t_2 = 30 ps in dodecane (blue and red boxes represent [ω_{UP}, ω_{LP}] and [ω_{UP}, ω_{MP}] peaks, respectively), along with the corresponding linear spectrum (top panel) and normalized narrowband pump probe spectrum at $\omega_1 = \omega_{UP}$ (bottom panel). (D) Experimental dynamics of cross peaks (top panel) and diagonal peaks (bottom panel) for $Fe(CO)_5$ outside the cavity upon pumping of the a_2" modes (red dots) and inside the cavity upon pumping of UP (blue dots) and the a_2" dark modes (gray dots). The black dashed, dotted and solid lines are the

corresponding fits. Energy is exchanged at a faster rate when pumping UP, whereas pumping the a_2" dark modes leads to a similar rate to the one outside the cavity.

We used 2D IR to monitor the cross-peak dynamics both outside and inside the cavity (*26-29*). Through pseudorotation and IVR, the a_2" and e' modes can exchange energy. By measuring the dynamics of the [2022, 1986] cross and [2022, 2010] diagonal peaks of the 1->2 transitions (Fig. S6) and fitting them to a kinetic model (see SM Section 2.3.1), we determined the energy exchange rate constant k_{ex} to be (0.084 ± 0.002) ps^{-1} at 25 °C (Fig. 1D). Here, unless specifically mentioned, all measurements were done under magic angle conditions to remove contributions from rotational dynamics.

Similarly, for $Fe(CO)_5$ under VSC (Fig. 1C, bottom), we followed the dynamics of the [ω_{UP}, ω_{MP}] (red box in Fig. 1C) and [ω_{UP}, ω_{LP}] (blue box in Fig. 1C) peaks of the 2D IR spectrum (or the corresponding narrowband pump probe spectra; see SI Section 1.3 for details). Here we specifically focus on the dynamics involving pumping UP, to avoid complications of hot (*i.e.*, highly excited) vibrational states when exciting LP modes (*30*). The interpretation of these peaks was discussed in our previous works (*27*). Basically, the polariton transitions at ω_{MP} and ω_{LP} overlap with the 1->2 transition of the a_2" and e' modes, respectively (this assignment is further confirmed by spectral simulations (SM Section 2.6) and input-output theory (SM Section 4)). Upon exciting UP, when the waiting time was beyond the polariton lifetime, the [ω_{UP}, ω_{MP}] and [ω_{UP}, ω_{LP}] peaks corresponded respectively to the excited state population of the a_2" and e' modes. Therefore, the dynamics of these peaks reported the energy transfer between the a_2" and e' modes facilitated by pseudorotation and IVR. At a first glance, the dynamics under VSC were a bit faster than the one without (Fig.1D).

To quantify the energy exchange dynamics upon pumping UP, we used the kinetic model shown in Fig.2A. First, the population of UP relaxed to both the a_2" and e' dark modes within the polariton lifetime. Then, the a_2" and e' dark modes exchanged energy, through pseudorotation and IVR, and at the same time dissipated energy to their environment. The solution of this kinetic model provided a good fit to the [ω_{UP}, ω_{MP}] and [ω_{UP}, ω_{LP}] dynamics (Fig.2B). Furthermore, the measured dynamics could be separated into three components: polariton relaxation to dark modes at short times (cavity leakage is implicitly accounted for; see SM Section 2.3.2), energy exchange at intermediate times, and vibrational decay at long times. From the fitted results, k_{ex} under VSC was 0.113 ± 0.009 ps^{-1} at room temperature, 30% faster than that outside the cavity.

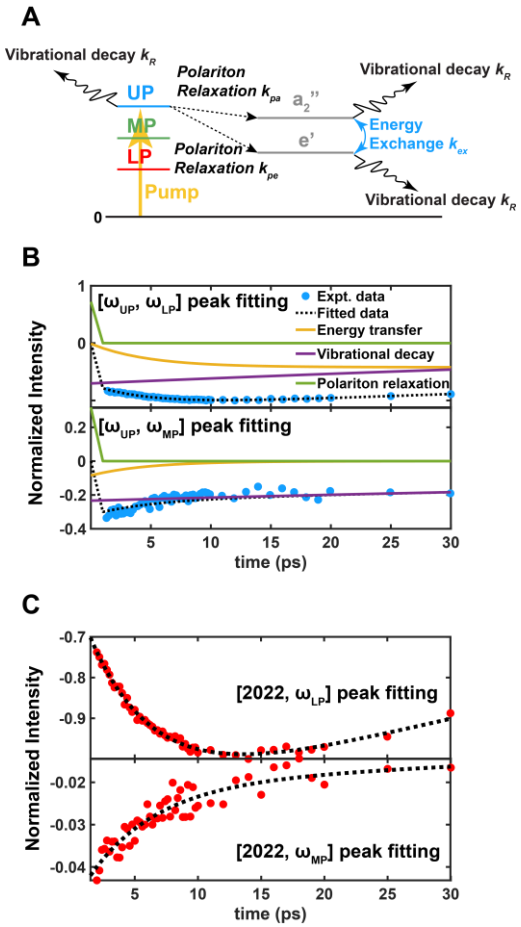

Fig 2 Energy exchange dynamics between a_2'' and e' modes. (A) Schematic drawing of the kinetic model for $Fe(CO)_5$ under VSC. See SI Section 2.3.2 for details of the kinetic model. (B) Experimental data (blue dots) and fits (black dotted lines) including each component for [ω_{UP}, ω_{LP}] (top panel) and [ω_{UP}, ω_{MP}] (bottom panel) peaks. (C) Experimental data (red dots) and fits (black dotted lines) for the [2022, ω_{LP}] (top panel) and [2022, ω_{MP}] (bottom panel) peaks when the a_2'' dark modes are pumped.

Using 2D IR and the same analysis, we found when exciting the a_2'' dark reservoir modes directly, the energy exchange dynamics had similar trends to those outside the cavity (Fig.2C), and k_{ex} was 0.090 ± 0.006 ps^{-1}. Clearly, VSC was only modifying the dynamics when the polaritons are pumped, whereas pumping the a_2'' dark reservoir modes caused the system to evolve similarly to the molecules outside the cavity, agreeing with the reservoir's purely molecular character. Similar findings have been predicted by a recent theoretical work (*31*). The contrast of dynamics between pumping UP and dark a_2'' modes suggests that the energy exchange rates depend on the initial populated states.

Although we have shown that VSC leads to faster energy exchange between the a_2" and e' modes, this acceleration could be due to enhancement of either pseudorotation or IVR. To qualitatively distinguish between the two processes, we could measure the vibrational anisotropy (*32*) associated with the cross peaks. IVR involved energy transfer between e' and a_2" modes perpendicular to each other (Fig.3A), and pseudorotation caused energy exchange between e' and a_2" modes parallel to each other (Fig.3B). Thus, the anisotropy should start from -0.2 and 0.4 for the former and latter (*32-34*), respectively. In general, both processes occurred concurrently, and the initial anisotropy lay between these values.

Outside the cavity, the initial value of anisotropy was ~0.06 for exciting the a_2" modes (Fig. 3C), suggesting that pseudorotation dominated over IVR. However, under VSC, the opposite trend was observed: the anisotropy started at ~-0.08 for exciting UP (Fig. 3D). This contrast indicates that, under VSC, IVR dominated over pseudorotation. Not surprisingly, when pumping the a_2" dark modes under VSC, the anisotropy was ~0.06 (Fig. S18), like the cavity-free case.

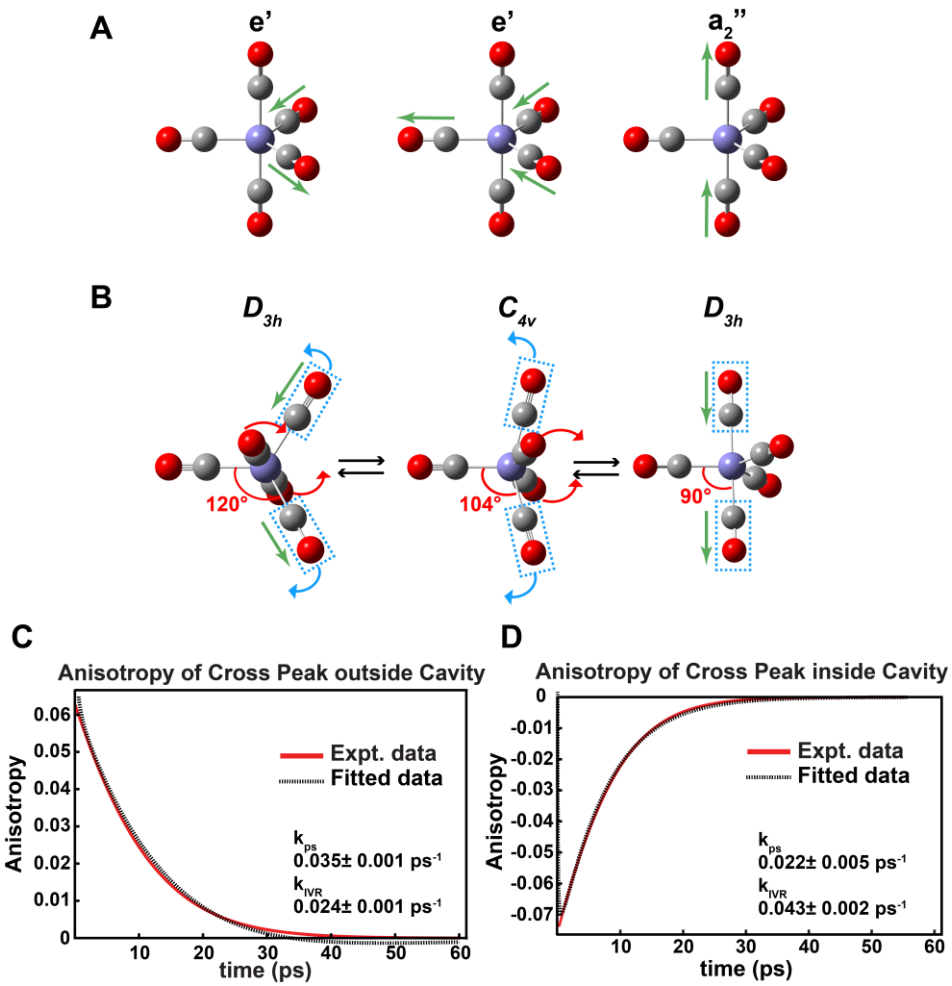

Fig. 3 Cross-peak anisotropy dynamics of IVR and pseudorotation. (A) Depiction of the eigenvectors for the a_2" and doubly degenerate e' vibrational modes of $Fe(CO)_5$. IVR leads to energy transfer between modes that are perpendicular to each other. (B) Pseudorotation leads to energy transfer between a_2" and e' modes that are parallel to each other. (C, D) Experimental anisotropy (red line) and corresponding fits (black dotted line) for cross peak of $Fe(CO)_5$ (C) outside the cavity ([2022, 1986]) and (D) under VSC ([ω_{UP}, ω_{MP}]). Listed are the rate constants, extracted from the fitting, of IVR (k_{IVR}) and pseudorotation (k_{ps}). The rate constants indicate that VSC accelerated IVR and suppressed pseudorotation.

To determine the rate constants of pseudorotation and IVR, a more detailed kinetic model was developed (see SM Section 2.4)(*32-34*).The anisotropy can be calculated based on the energy exchange dynamics simulated from the kinetic model. Fitting the measured anisotropy dynamics to the kinetic model, we determined the rate constants for pseudorotation (k_{ps}) and IVR (k_{IVR}) to be 0.035±0.001 and 0.024±0.001 ps^{-1}, respectively, outside the cavity (Fig. 3C) and 0.022±0.005 and 0.043±0.002 ps^{-1} under VSC (Fig. 3D). The former results qualitatively agree with previous

work showing that pseudorotation dominated the dynamics outside a cavity(*23*), except now we quantified the relative contribution of IVR. The quantitative results agreed with the qualitative analysis above, indicating that VSC shifted the balance between pseudorotation and other energy exchange channels: outside the cavity, exciting the a_2" mode yielded dynamics where pseudorotation dominated over IVR, and under VSC, exciting the UP promoted IVR and suppressed pseudorotation; yet, under VSC, exciting the a_2" dark modes did not change the dynamics relative to molecules outside the cavity. We note that this effect is VSC-exclusive, as weak coupling to the cavity did not lead to the modification of the dynamics (SM section 3.4); further, the acceleration of energy transfer and promotion of IVR through VSC was robust against different solvent environments (see results for 1-octanol ,SM Section 3.9).

The sharp contrast between the VSC dynamics starting in UP and a_2" dark reservoir modes is interesting because, even when UP was excited, the population relaxed to the dark modes on a much shorter time scale than pseudorotation and IVR. The difference then lies in the relaxation processes available to the initial states. Several mechanisms could explain the faster IVR upon pumping UP. For example, the decay from UP to the a_2" dark modes was accompanied by excitation of low-frequency vibrations (*i.e.*, phonons), and some of these phonons could be further excited during the energetically downhill IVR from a_2" to e' modes. It follows that IVR would be accelerated by the first scattering process, and this enhancement would not occur if the system were initialized in the a_2" dark modes. A limitation of this hypothesis is that, at room temperature, the phonons should have a high occupation number ($\approx$10), which should not change significantly when UP relaxes to dark modes (through one- or few-phonon excitation). Another possibility is that the VSC-induced speedup in the dynamics reflects a polariton-induced intermolecular vibrational energy transfer. In this case though, the observed anisotropy dynamics should practically be zero, or have a fast decay(*27*), instead of starting from a negative value, due to the lack of orientational correlation between donor and acceptor molecules. On the other hand, the mild suppression of pseudorotation is surprising, as it is conventionally thought that these high frequency vibrational modes do not drive the reaction. However, the co-existence of IVR enhancement and pseudorotation suppression suggests otherwise. By quickly going through IVR, molecules may lose their driving force for pseudorotation, leading to its slowdown. It is also possible that the pseudorotation motion is hindered by the phonons excited by the transition from UP to the dark modes. The temperature-dependent measurements further showed that VSC shifts the thermodynamic parameters of activation in the same direction (SM Section 2.4), which has also been observed—and rather consistently—in reports of reaction kinetics altered by VSC(*30*). This correspondence supports that the insights obtained here should be relevant to understanding the previous experiments(*35*).

Using 2D IR to resolve ultrafast chemical dynamics with specific initial states, we quantified the energy exchange dynamics in $Fe(CO)_5$ under VSC. We showed that when UP was excited under VSC, IVR was promoted and pseudorotation was suppressed compared to the bare molecular system. However, pumping the dark reservoir modes under VSC led to little change in the dynamics compared to outside the cavity. Because the population at thermal equilibrium resided predominantly in the dark modes, the overall influence of VSC on $Fe(CO)_5$ should be negligible without external (*e.g.*, laser) pumping. Yet, the present results show an important insight to unify the works reporting VSC-modified reactions and the ones reporting or predicting the opposite – regardless of how reactions behave under thermally-activated conditions, the basic concept of VSC-modified chemistry works: populated polaritons can influence chemical dynamics. These findings suggest that the future of VSC-modified thermal chemistry lies in

controlling the dark modes, with either reducing the number of dark reservoir modes, *e.g.*, through cavity miniaturization, or making dark modes more delocalized through heterogeneity(*36-38*).

References and Notes

1. J. P. Long, B. S. Simpkins, *ACS Photonics* **2**, 130-136 (2015).
2. A. Shalabney *et al.*, *Nat. Commun.* **6**, 1-6 (2015).
3. T. W. Ebbesen, *Acc. Chem. Res.* **49**, 2403-2412 (2016).
4. A. Thomas *et al.*, *Angew. Chem. Int. Ed.* **55**, 11462-11466 (2016).
5. A. Thomas *et al.*, *Science* **363**, 615-619 (2019).
6. K. Hirai, R. Takeda, J. A. Hutchison, H. Uji-i, *Angew. Chem. Int. Ed.* **59**, 5332-5335 (2020).
7. Y. Pang *et al.*, *Angew. Chem. Int. Ed.* **59**, 10436-10440 (2020).
8. F. J. Garcia-Vidal, C. Ciuti, T. W. Ebbesen, *Science* **373**, eabd0336 (2021).
9. A. Sau *et al.*, *Angew. Chem. Int. Ed.* **60**, 5712-5717 (2021).
10. J. A. Campos-Gonzalez-Angulo, R. F. Ribeiro, J. Yuen-Zhou, *Nat. Commun.* **10**, 1-8 (2019).
11. J. Galego, C. Climent, F. J. Garcia-Vidal, J. Feist, *Phys. Rev. X* **9**, 021057 (2019).
12. T. E. Li, A. Nitzan, J. E. Subotnik, *J. Chem. Phys.* **152**, 234107 (2020).
13. I. Vurgaftman, B. S. Simpkins, A. D. Dunkelberger, J. C. Owrutsky, *J. Phys. Chem. Lett.* **11**, 3557-3562 (2020).
14. V. P. Zhdanov, *Chem. Phys.* **535**, 110767 (2020).
15. M. Du, J. A. Campos-Gonzalez-Angulo, J. Yuen-Zhou, *J. Chem. Phys.* **154**, 084108 (2021).
16. M. V. Imperatore, J. B. Asbury, N. C. Giebink, *J. Chem. Phys.* **154**, 191103 (2021).
17. X. Li, A. Mandal, P. Huo, *Nat. Commun.* **12**, 1315 (2021).
18. J. A. Campos-Gonzalez-Angulo, J. Yuen-Zhou, *J. Chem. Phys.* **156**, 194308 (2022).
19. J. A. Campos-Gonzalez-Angulo, J. Yuen-Zhou, *J. Chem. Phys.* **152**, 161101 (2020).
20. T. E. Li, A. Nitzan, J. E. Subotnik, *J. Chem. Phys.* **154**, 094124 (2021).
21. G. D. Wiesehan, W. Xiong, *J. Chem. Phys.* **155**, 241103 (2021).
22. R. S. Berry, *J. Chem. Phys.* **32**, 933-938 (1960).
23. J. F. Cahoon, K. R. Sawyer, J. P. Schlegel, C. B. Harris, *Science* **319**, 1820-1823 (2008).
24. F. H. Westheimer, *Acc. Chem. Res.* **1**, 70-78 (1968).
25. P. Törmä, W. L. Barnes, *Rep. Prog. Phys.* **78**, 013901 (2014).
26. B. Xiang *et al.*, *Proc. Natl. Acad. Sci. U.S.A.* **115**, 4845-4850 (2018).
27. B. Xiang *et al.*, *Science* **368**, 665-667 (2020).
28. B. Xiang, J. Wang, Z. Yang, W. Xiong, *Sci. Adv.* **7**, eabf6397 (2021).
29. B. Xiang, W. Xiong, *J. Chem. Phys.* **155**, 050901 (2021).
30. B. Xiang *et al.*, *J. Phys. Chem. A* **123**, 5918-5927 (2019).
31. D. Wellnitz, G. Pupillo, J. Schachenmayer, *Commun. Phys.* **5**, 1-11 (2022).
32. R. M. Hochstrasser, *Chem. Phys.* **266**, 273-284 (2001).
33. A. Tokmakoff *et al.*, *J. Chem. Phys.* **102**, 3919-3931 (1995).
34. P. Hamm, M. Zanni, *Concepts and methods of 2D infrared spectroscopy*. (Cambridge University Press, 2011).
35. A. D. Dunkelberger, B. S. Simpkins, I. Vurgaftman, J. C. Owrutsky, *Annu. Rev. Phys. Chem.* **73**, 429-451 (2022).
36. T. Botzung *et al.*, *Phys. Rev. B* **102**, 144202 (2020).

37. G. D. Scholes, *Proc. R. Soc. A* **476**, 20200278 (2020).
38. M. Du, J. Yuen-Zhou, *Phys. Rev. Lett.* **128**, 096001 (2022).
39. M. Khalil, N. Demirdöven, A. Tokmakoff, *J. Phys. Chem. A* **107**, 5258-5279 (2003).
40. D. V. Kurochkin, S. R. G. Naraharisetty, I. V. Rubtsov, *Proc. Natl. Acad. Sci. U.S.A.* **104**, 14209-14214 (2007).
41. P. Saurabh, S. Mukamel, *J. Chem. Phys.* **144**, 124115 (2016).
42. Z. Yang, B. Xiang, W. Xiong, *ACS Photonics* **7**, 919-924 (2020).
43. C. A. DelPo *et al.*, *J. Phys. Chem. Lett.* **11**, 2667-2674 (2020).
44. G. Khitrova, H. M. Gibbs, F. Jahnke, M. Kira, S. W. Koch, *Rev. Mod. Phys.* **71**, 1591 (1999).
45. J. A. Campos-Gonzalez-Angulo, R. F. Ribeiro, J. Yuen-Zhou, *New. J. Phys.* **23**, 063081 (2021).
46. A. D. Dunkelberger, R. B. Davidson, W. Ahn, B. S. Simpkins, J. C. Owrutsky, *J. Phys. Chem. A* **122**, 965-971 (2018).
47. B. Xiang *et al.*, *Sci. Adv.* **5**, eaax5196 (2019).
48. R. Houdré, R. P. Stanley, M. Ilegems, *Phys. Rev. A* **53**, 2711 (1996).
49. R. Duan, J. N. Mastron, Y. Song, K. J. Kubarych, *J. Phys. Chem. Lett.* **12**, 11406-11414 (2021).
50. R. F. Ribeiro *et al.*, *J. Phys. Chem. Lett.* **9**, 3766-3771 (2018).

Acknowledgments: The authors thank Harsh H. Bhakta for assisting with the Mathematica code. **Funding:** T.-T.C. is supported by National Science Foundation DMR-1848215. Z.Y. is supported by AFSOR FA9550-21-1-0369. W.X. thanks the general support for summer salaries from Alfred P. Sloan Foundation FG-2020-12845 and National Science Foundation CHE-2101988. Acknowledgement is made to the donors of The American Chemical Society Petroleum Research Fund for M.D.'s support of this research through the ACS PRF 60968-ND6 Grant. J.Y.-Z. was supported by the US Department of Energy, Office of Science, Basic Energy Sciences, CPIMS Program under Early Career Research Program Award DE-SC0019188. **Author contributions:** W. X. conceived the original idea and supervised the overall research. T.-T.C. ,Z.Y. and W.X. designed the experiments. T.-T.C. and Z.Y. conducted the experimental work. T.-T.C., M.D., J.Y.-Z. and W.X. analyzed data. M.D. and W.X. developed the anisotropy model. M.D. and J.Y.-Z. proposed mechanisms and developed spectral theory in SI section 4. T.-T.C. M.D., J.Y.-Z. and W.X. interpreted the results and wrote the manuscript. **Competing interests:** None declared. **Data and materials availability:** All (other) data needed to evaluated the conclusions in the paper are present in the paper or the Supplementary Materials.

Commented [XW1]: Cite the repository link here

Supplementary Materials

Materials and Methods

Supplementary Text

Figs. S1 to S44

Tables S1 to S7

References (20, 23, 25-30, 32-34, 39-50)